

Phase-Locked Loops- A Broad Perspective Continued

1 Introduction

In Part 1 of this article, we looked at a number of phase-locked loop (PLL) concepts ranging from continuous and sampled control systems to estimation theory based perspectives. In Part 2, we will continue our examination of the PLL concept in the estimation theory sense by looking at maximum a posteriori (MAP) based PLLs and the fundamental performance limits described by the Cramer-Rao bound. Our theoretic involvement will culminate with a Kalman filtering perspective for the PLL. The balance of this article will utilize the PLL concept in several real-world applications.

2 Maximum a Posteriori (MAP) Based Estimators

The MAP estimator form is used for the estimation of random parameters whereas the maximum-likelihood (ML) form is generally associated with the estimation of deterministic parameters. From Bayes Rule, we know that given an observation z that

$$(1) \quad p(\theta|z) = \frac{p(z|\theta)p(\theta)}{p(z)}$$

and this can be re-written in the logarithmic form as

$$(2) \quad \text{Ln}[p(\theta|z)] = \text{Ln}[p(z|\theta)] + \text{Ln}[p(\theta)] - \text{Ln}[p(z)]$$

This log-probability may be maximized by setting the derivative with respect to θ to zero thereby creating the necessary condition that¹

$$(3) \quad \frac{d}{d\theta} \{ \text{Ln}[p(z|\theta)] + \text{Ln}[p(\theta)] \}_{\theta=\hat{\theta}_{MAP}} = 0$$

If the density $p(\theta)$ is not known, we are forced to ignore the second term in (3) which leads naturally to the maximum-likelihood form as

$$(4) \quad \frac{d}{d\theta} \{ \text{Ln}[p(z|\theta)] \}_{\theta=\hat{\theta}_{ML}} = 0$$

¹ [13] and [14] Section 6-2.1; [20] Section 5.4; [21] Section 2.4.1

Although the MAP and ML estimators are not the same in the strict sense, the MAP estimator takes on the form of the ML estimator in the absence of sufficient prior knowledge of θ .

The similarities between the MMSE, ML, and MAP estimators should not go unnoticed. In the Gaussian noise case where the observed signal is given by

$$(5) \quad z(t) = y(t, \theta) + v(t) \quad \text{for } t_o \leq t \leq t_f$$

in which $v(t)$ is the noise and θ is the nonrandom parameter of interest, it can be shown that the maximum-likelihood (ML) estimate for θ is given by

$$(6) \quad \int_{t_o}^{t_f} [z(t) - y(t, \theta)] \frac{\partial y(t, \theta)}{\partial \theta} dt \Big|_{\theta = \hat{\theta}_{ML}} = 0$$

In the jointly Gaussian case where θ is assumed to be a random parameter having a variance of σ_θ^2 , use of (3) leads to the result that

$$(7) \quad \hat{\theta}_{MAP} = \frac{2}{N_o} \sigma_\theta^2 \int_{t_o}^{t_f} [z(t) - y(t, \theta)] \frac{\partial y(t, \theta)}{\partial \theta} dt \Big|_{\theta = \hat{\theta}_{MAP}}$$

These two results illustrate how similar the ML and MAP estimates can appear.

The Fundamental Theorem of Estimation Theory [22] states that the estimator that minimizes the mean-square error is given by

$$(8) \quad \hat{\theta}_{opt} = E[\theta | z]$$

It can also be shown that the best linear unbiased estimator (BLUE) form takes on the form of the weighted least-squares estimator given that the proper samples weighting is applied.

In Part I of this article, we found that the ML estimator for the signal phase utilized a gradient error metric that sought to drive any quadrature (or orthogonal) signal components to zero. This is not unlike the Orthogonality Principle in estimation theory which stipulates that any residual estimation error should be orthogonal (i.e., uncorrelated) with the observations as

$$(9) \quad E[(\hat{\theta} - \theta)z] = 0$$

In summarizing this section on estimation theory, the following summary may be helpful [21]:

-
-
- The minimum mean-square error estimate is always the mean of the a posteriori density (the conditional mean).
 - The MAP estimate is the value of θ at which the a posteriori density has its maximum.
 - For a large class of cost functions the optimum estimate is the conditional mean whenever the a posteriori density is a unimodal function which is symmetric about the conditional mean.
 - ML estimates are consistent, asymptotically Gaussian, and asymptotically efficient.
 - The ML estimate is the value of θ that maximizes the conditional density $p(z|\theta)$ for nonrandom parameter θ , and if any estimate exists that achieves the Cramer-Rao Bound (See Section 3), it will be equal to the ML estimate.

More information on the fundamentals of estimation theory can be found in [20,21,22].

3 Performance Limits From the Cramer-Rao Bound

In the case of unbiased estimators for nonrandom parameters, the Cramer-Rao Bound (CRB) provides a lower-bound for the estimation error variance achievable. One of the most important aspects of the CRB and bounds like it is that the difficulty of a given design objective can be very quickly judged by comparing a given requirement with the appropriate bound. In other words, it can be embarrassing to find out after already expending a great deal of time and effort on a problem that the requirement runs contrary to the laws of physics.

In the single-parameter case, the CRB is usually presented in two different equivalent forms as [20,21,22]

$$(10) \quad \text{var}[(\hat{\theta} - \theta)|\theta] = E[(\hat{\theta} - \theta)^2|\theta] \geq \left\{ E \left[\left[\frac{\partial \ln p(z|\theta)}{\partial \theta} \right]^2 | \theta \right] \right\}^{-1}$$

$$\text{var}[(\hat{\theta} - \theta)|\theta] \geq - \left\{ E \left[\frac{\partial^2 \ln p(z|\theta)}{\partial \theta^2} | \theta \right] \right\}^{-1}$$

When multiple parameters are being estimated (e.g., amplitude, phase, frequency), the CRB takes the form of the Fisher Information Matrix. The interested reader should consult [19,20,21,22] for additional information on this topic.

It is of interest to compare the MAP and PLL phase estimators in terms of some performance measures. In order to do this, we first obtain the variance of each estimator. As developed in Section 5.1.2, the steady-state first-order (and second-order) PLL phase estimator probability density is taken to be the Tikhonov probability density

function that is given by

$$(11) \quad p(\hat{\theta} - \theta) = \frac{\exp[\alpha \cos(\hat{\theta} - \theta)]}{2\pi I_0(\alpha)}$$

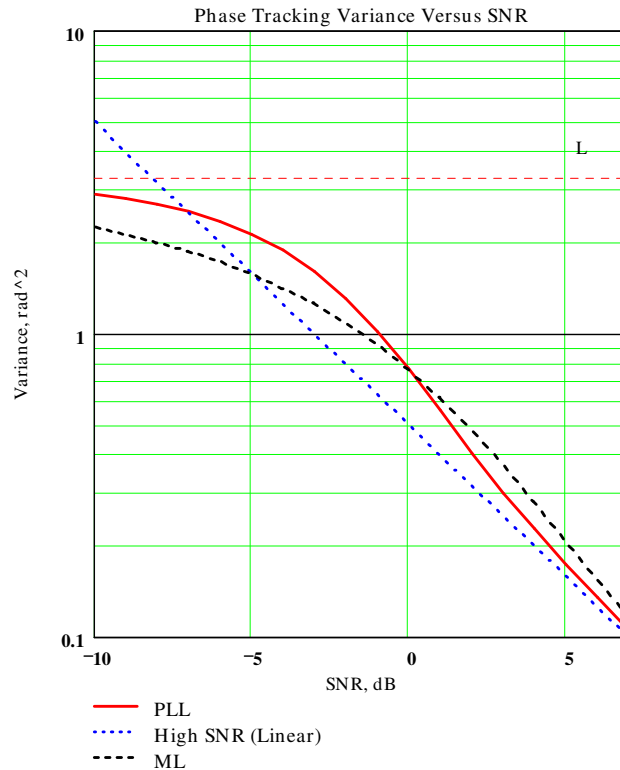
where $I_0()$ is the zeroth-order modified Bessel function of the first kind and α is the SNR within the PLL. The variance for the PLL estimator is given by [13]

$$(12) \quad \sigma_{PLL}^2 = \frac{\pi^2}{3} + 4 \sum_{n=1}^{\infty} \frac{(-1)^n I_n(\alpha)}{n^2 I_0(\alpha)}$$

These results and the linear result in which $\sigma_{\theta}^2 = \alpha^{-1}$ are plotted for comparison purposes in Figure 1.

When confronted with a phase, frequency, amplitude or combination of parameters estimation problem, designers should immediately evaluate how close the requirement is to the CRB. This step provides invaluable insight into (i) whether the task is even achievable, and (ii) the difference between the requirement and theory is a true measure of the design difficulty involved.

Figure 1 Tracking Variance for MAP and PLL Phase Estimators Versus SNR



4 Optimal Mean-Square-Error Tracking: Kalman Filtering

The phase-locked loop can be cast as an extended Kalman filter and hence it is an approximate solution for the optimal nonlinear filtering problem [9]. The Kalman filter is a set of mathematical equations that provides an efficient recursive means to estimate the state \underline{x} of a process, in a way that minimizes the mean of the squared error. The filter is very powerful in several aspects: it supports estimation of past, present and even future events [10].

The Kalman filter addresses the general problem of trying to estimate the state \underline{x} of a discrete-time controlled process that is governed by the linear stochastic difference equation of the form

$$(13) \quad \underline{x}_{k+1} = A\underline{x}_k + B\underline{u}_k + \underline{w}_k$$

with measurements given by

$$(14) \quad \underline{z}_{k+1} = H\underline{x}_{k+1} + \underline{v}_k$$

The A, B, and H matrices can be time-variable but are shown here as constant. The random vectors \underline{w}_k and \underline{v}_k represent the process and measurement noise respectively, and they are assumed to be statistically independent with covariance matrices Q and R respectively. Vector \underline{u}_k is the input to the system.

The mean-squared filtered estimate of the system state at time k+1 is represented by $\hat{\underline{x}}(k+1|k+1)$, and it can be written in predictor-corrector form as shown in Figure 2.

The similarities of the Kalman filter with other time-stationary results are striking. In the case of the BLUE, its recursive structure may be written in an almost identical form except that we have no time prediction steps since we have access to no system state information for the BLUE. Its formulation is shown in Figure 3.

The recursive Kalman equations lend themselves very easily to implementation within a second-order digital phase-locked loop (DPLL). This has been done before in [11] and [12].

Although the Kalman filter requires current information about the noise covariance in its execution through the Q and R matrices, it is particularly adept at improving the tracking performance in situations which are not time-stationary. As the structure content of the signal being tracked increases, the Kalman filter can deliver substantial performance gains over other methods which do not exploit state estimation.

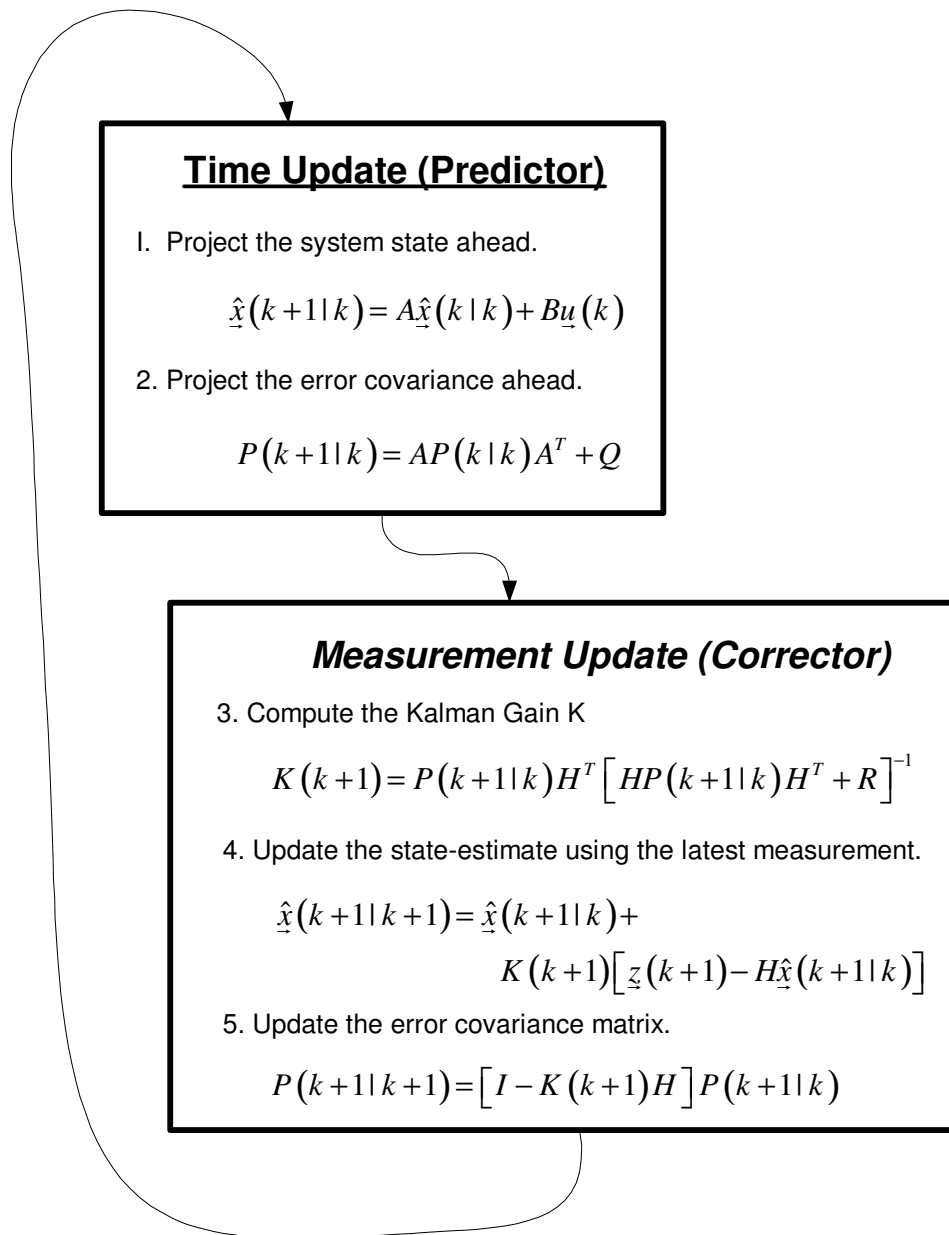
Figure 2 Organization of Kalman Filter as a Predictor-Corrector Sequence [10]

Figure 3 Recursive Equation Formulation for BLUE***Best Linear Unbiased Estimate (BLUE)***

$$\hat{\underline{\theta}}_{BLUE}(k+1) = \hat{\underline{\theta}}_{BLUE}(k) + K_{BLUE}(k+1) \left[\underline{z}(k+1) - H \hat{\underline{\theta}}_{BLUE}(k) \right]$$

$$K_{BLUE}(k+1) = P(k+1) H R^{-1}$$

$$P^{-1}(k+1) = P^{-1}(k) + H^T R^{-1} H$$

5 PLL Applications

5.1 RF Frequency Synthesis Using Charge-Pump Based PLLs

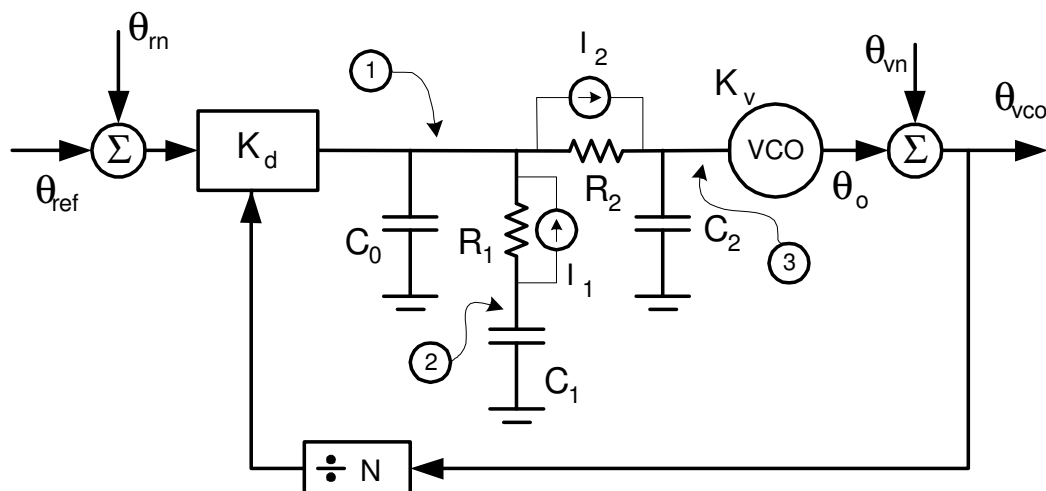
The National Semiconductor line of *Platinum*[™] frequency synthesizer devices revolutionized the world of frequency synthesis in the early 1990's by delivering unprecedented predictably-reliable phase noise performance in a highly-integrated low-cost device. These devices had a host of very nice features about them, but most notable was the low phase noise performance of the charge-pump phase detector along with the very low reference spur levels achievable. The excellent balance and leakage characteristics of the phase detector made it possible to implement a complete PLL with a very modest loop filter.

5.1.1 Classic Type-2 Charge-Pump Implementation

The circuit schematic for the classic type-2 4th-order PLL is shown here in Figure 4. The current noise sources associated with each resistor are shown shunted across each respective resistor, and the reference-related and VCO self-noise make up the remainder of the major noise contributors.

The normal approach that is taken to analyze this kind of system is to solve the nodal equations for the appropriate transfer functions algebraically as done in [4]. A streamlined approach is taken here where the same nodal equations are used but the

Figure 4 Circuit Diagram for Type-2 4th-Order PLL Using Charge-Pump Phase Detector. Phase Noise and Johnson Resistor Noise Sources All Shown.



customary algebraic manipulations are avoided by using matrix methods. The matrix equation that describes the circuit in Figure 4 can be quickly written down in Laplace transform form as

$$(15) \quad \begin{bmatrix} sC_0 + G_1 + G_2 & -G_1 & -G_2 & \frac{K_d}{N} \\ -G_1 & sC_1 + G_1 & 0 & 0 \\ -G_2 & 0 & G_2 + sC_2 & 0 \\ 0 & 0 & -\frac{K_v}{s} & 1 \end{bmatrix} \begin{bmatrix} V_1 \\ V_2 \\ V_3 \\ \theta_{VCO} \end{bmatrix} = \begin{bmatrix} I_1 - I_2 + K_d \theta_m \\ -I_1 \\ I_2 \\ \theta_{vn} \end{bmatrix}$$

where $G_i = (R_i)^{-1}$ and the I_j represent the Johnson current noise sources associated with each resistor. Analysis tools like Matlab and Mathcad can be used to numerically solve this equation for the transfer functions of interest and for closed-loop noise performance quantities. The noise current for the j^{th} resistor is given as

$$I_j = \sqrt{\frac{4kT_o}{R_j}}$$

and all of the noise sources are assumed to be statistically independent.

The phase detector referenced phase noise floor for the National Semiconductor *Platinum*TM series devices is given by

$$(16) \quad L_{PD} = L_{Floor} + 20 \text{Log}_{10}(F_{VCO}) - 10 \text{Log}_{10}(F_{REF})$$

where $L_{Floor} = -205 / -210 / -211 / -218$ dBc/Hz for the LMX2315/ LMX2306/ LMX2330 / LMX2346 devices respectively. This model or another can be used for the reference noise level represented in (15) by θ_m . Leeson's model can be similarly used for the VCO self-noise term represented by θ_{vn} in (15), recognizing that this noise contribution is frequency-dependent as given by

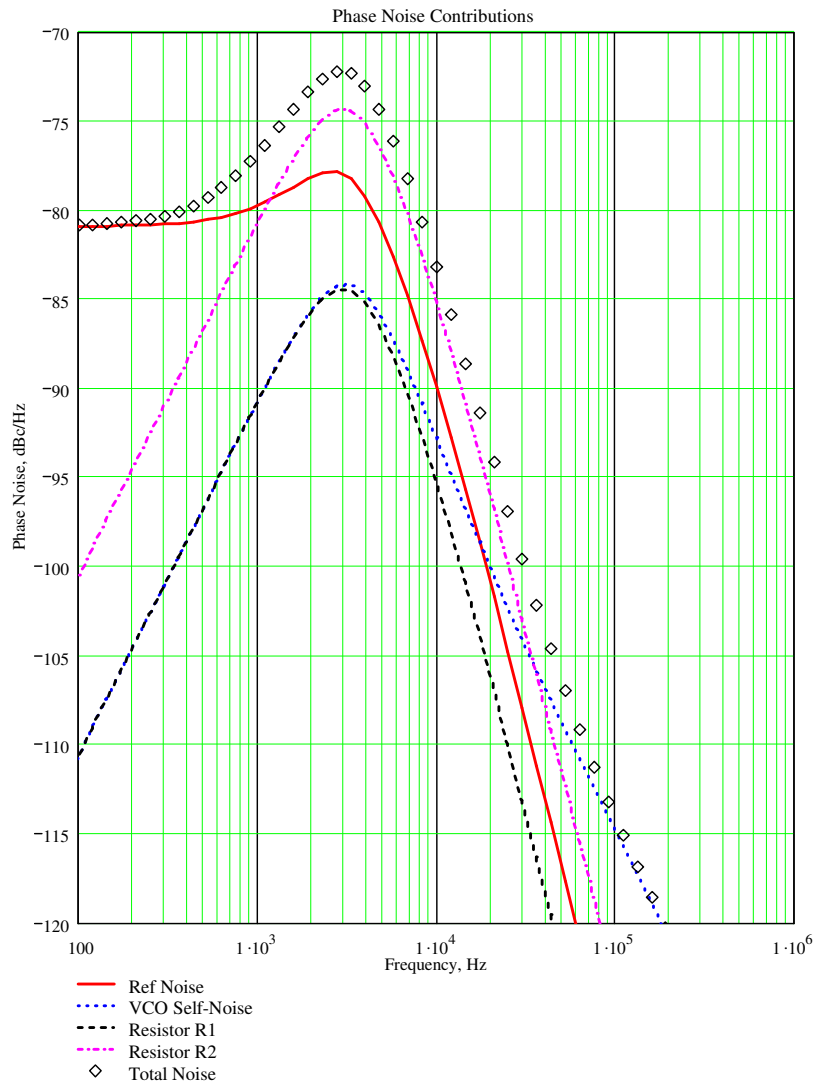
$$(17) \quad L_{VCO}(f) = 10 \text{Log}_{10} \left[\frac{FkT_o}{2P_o} \left(1 + \left(\frac{F_c}{2Q_L f} \right)^2 \right) \right]$$

in which F is noise factor, k is the Boltzmann's constant, $T_o = 290$ degrees Kelvin, P_o is the power extracted from the actual resonator in Watts, F_c is the VCO center frequency in Hz, and Q_L is the loaded resonator Q-factor. Additional terms are often added within the parenthesis to account for $1/f$ noise, etc., but these rarely survive the closed-loop action of the PLL and have consequently not been included here. A more complete discussion of oscillator noise and its modeling can be found in [5].

The transient response of the PLL to a step-change in phase or frequency can be

similarly computed using numerical techniques. The approach taken here is to substitute the Laplace transform of a step-frequency error given by $2\pi\Delta F/s^2$ in for θ_{vn} in (15), and then compute the Fourier transform for θ_{vco} at an equally-spaced grid of frequencies from which the inverse FFT provides the time-domain response. An example time-domain response is shown here in Figure 6. The ensuing details for both of these example results have purposely been omitted for brevity whereas they can be found on-line [6].

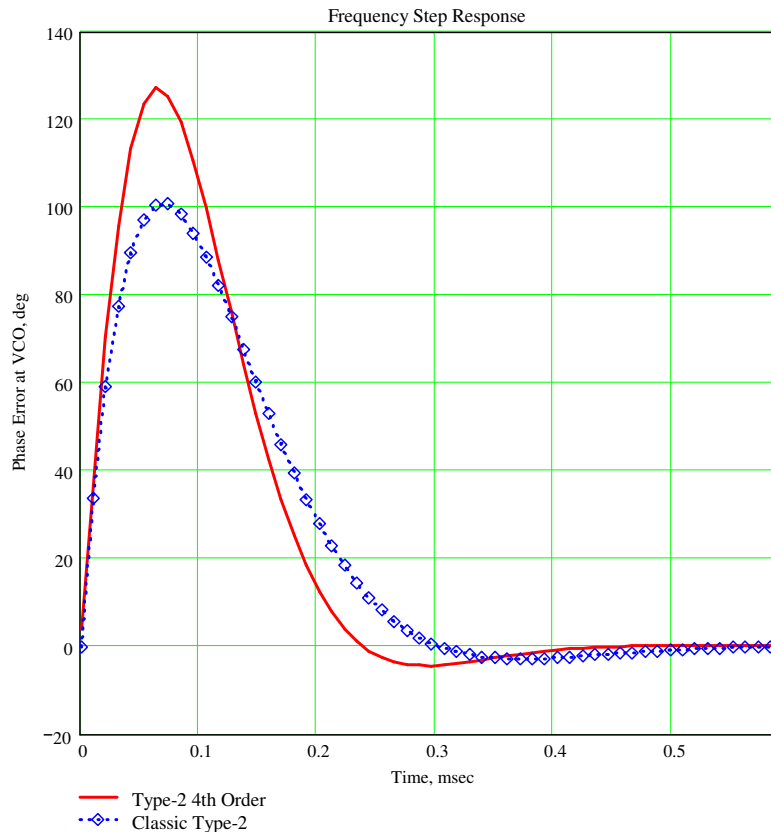
Figure 5 Example Noise Computation Using Matrix Methods



Several design procedures are available for designing “optimal” PLL loop filters. Whenever the word *optimal* is used however, designers should ask the question, “Optimal with respect to what criteria?” Some communication systems are primarily concerned with frequency error whereas others are concerned with phase error. If the wrong criteria is adopted, the design can often result in being more difficult than necessary. It is therefore very attractive to have an interactive tool that permits a

simultaneous examination of both the time as well as output spectrum domains.

Figure 6 Example Time-Domain Response to Step-Frequency Change Using FFTs



5.1.2 Phase Noise Impact on Communication Systems

Phase noise manifests itself in primarily two undesired phenomenon when it comes to wireless communications and frequency synthesis. Close-in² phase noise interferes with coherence in the receiver and in the case of QAM signal constellation, causes adjacent constellation points to be received more likely in error when channel noise is present. (Amplitude noise at the output of a properly designed synthesizer should be 20 dB or more below the phase noise level, and is therefore rarely a consideration.) In frequency-modulated systems, the phase noise can be equivalently expressed as a residual FM noise and it similarly adds to confusion in the receiver as to which frequency was truly sent by the transmitter. Far-out phase noise degrades channel selectivity, adjacent channel occupancy, and receiver third-order intercept point due to reciprocal mixing. Only a few of the most common digital communication

² Phase noise that falls at frequency offsets between roughly 0.01 times the symbol rate and 0.5 times the symbol rate

waveforms will be considered here due to space limitations.

The close-in phase noise impairment to (uncoded) bit error rate performance is most often computed using the Tikhonov probability distribution function for the noise. For large signal-to-noise ratio (SNR) arguments, numerical evaluation of the zeroth-order Bessel function can become problematic and it is more convenient to closely approximate this density function as

$$(18) \quad p_{\theta}(\theta, \sigma_{\theta}^2) \approx \sqrt{\frac{1}{2\pi\sigma_{\theta}^2}} \exp\left[\frac{\cos(\theta)-1}{\sigma_{\theta}^2}\right]$$

in which σ_{θ}^2 is the variance of the phase noise process involved. This variance is normally calculated as

$$(19) \quad \sigma_{\theta}^2 = 2 \int_{F_L}^{F_s} L(f) df$$

where $L(f)$ is the phase noise power spectral density of the local oscillators involved in rad^2/Hz , F_s is the symbol rate, and F_L is a lower frequency limit normally given as $0.01 F_s$ or thereabouts, depending upon the carrier-recovery baseband processing that may be present in the complete system. These definitions apply for a single-carrier system but need some additional enlargement in the case of multi-carrier systems like OFDM. In the case of QAM-style digital modulations, the (uncoded) symbol error rate can then be computed as

$$(20) \quad P_{SER}\left(\frac{E_s}{N_o}, \sigma_{\theta}\right) = \int_{-\pi}^{+\pi} P_S\left(\frac{E_s}{N_o}|\theta\right) p(\theta, \sigma_{\theta}^2) d\theta$$

Some results computed in this manner may be found in [8]. The conditional symbol-error-rate formulas for coherent BPSK and QPSK performance are respectively given as

$$(21) \quad P_{SER_BPSK}\left(\frac{E_b}{N_o}|\theta\right) = \frac{1}{2} \text{erfc}\left[\sqrt{\frac{E_b}{N_o}} \cos(\theta)\right]$$

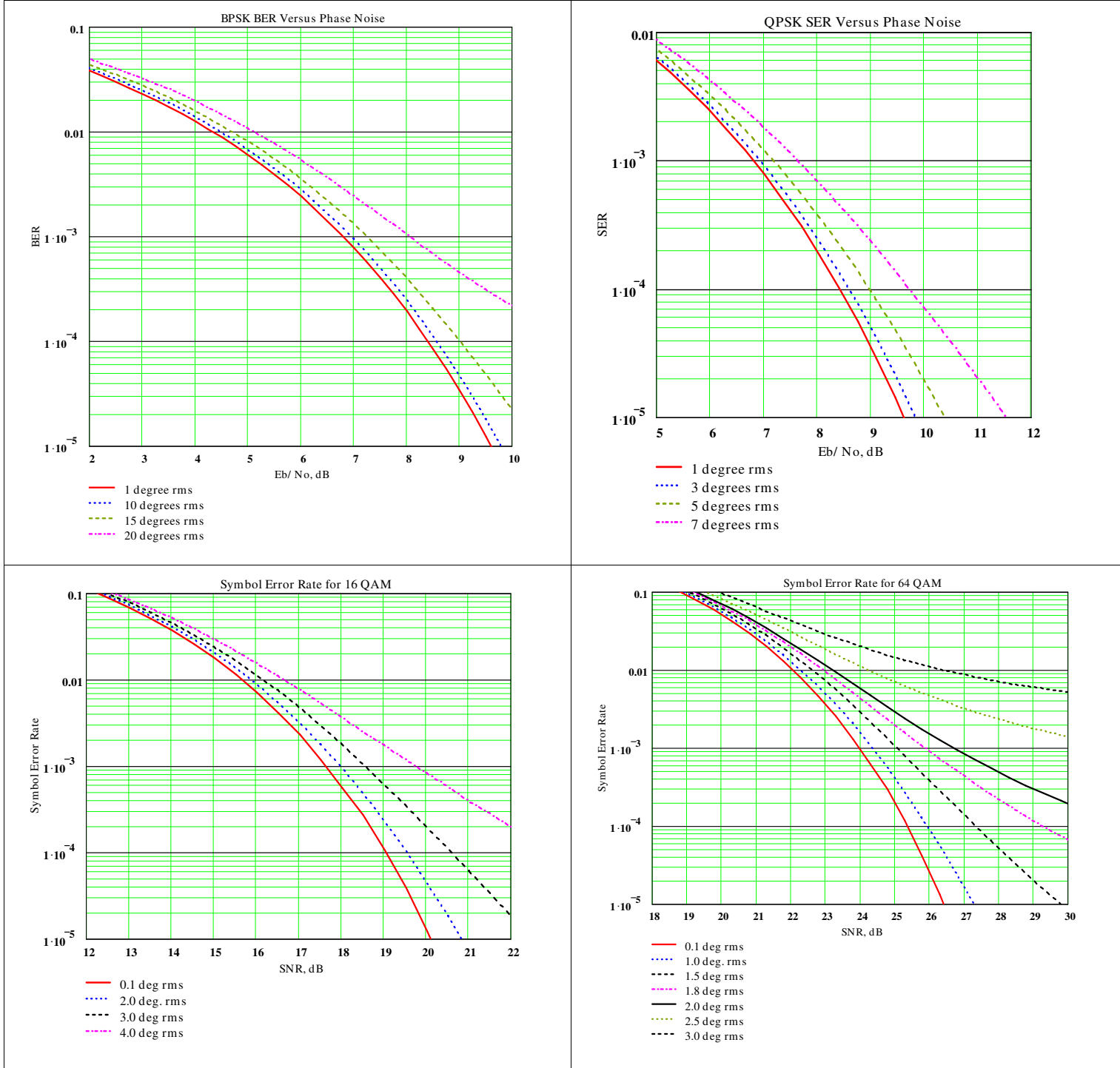
$$(22) \quad P_{SER_QPSK}\left(\frac{E_b}{N_o}|\theta\right) = \frac{1}{4} \text{erfc}\left\{\sqrt{\frac{E_b}{N_o}} [\cos(\theta) - \sin(\theta)]\right\} + \frac{1}{4} \text{erfc}\left\{\sqrt{\frac{E_b}{N_o}} [\cos(\theta) + \sin(\theta)]\right\}$$

The conditional symbol error rate relationships for other square-QAM signal constellations like 64-QAM can be found in [7].

It should come as no surprise that BPSK shows little susceptibility to phase noise related performance loss as shown in Table 1 since it is essentially an amplitude-based

modulation type. Performance degrades significantly as the signal constellation size increases, culminating in sub-one degree rms phase noise being desirable for 64-QAM in order to avoid appreciable E_b/N_o loss.

Table 1 QAM Uncoded Symbol Error Rate with Phase Noise



Phase noise performance can often set the achievable limit for the residual bit-error rate in a system.

In the case of carrier-recovery in which coherent demodulation is to be performed on QAM-type signals, the Costas loop has found wide-spread use as an unbiased low-variance practical solution. It can be shown that the Costas loops for BPSK and QPSK are equivalent to 2nd and 4th power nonlinearities followed by a PLL. Block diagrams for the BPSK and QPSK Costas loops are shown in Figure 7 and Figure 8 respectively.

Figure 7 MAP-Based Costas Carrier Recovery PLL for BPSK[14]

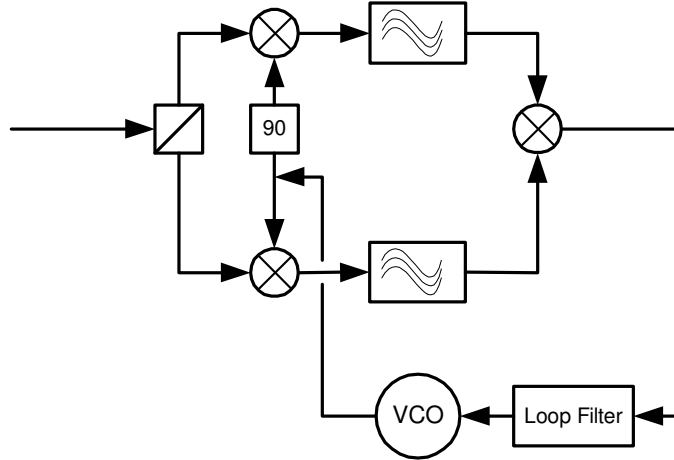
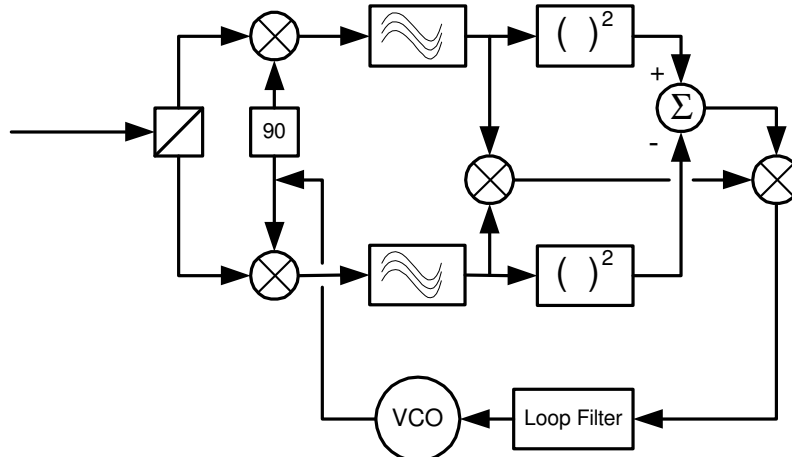


Figure 8 MAP-Based Carrier Recovery PLL for QPSK [15]



5.2 Symbol Timing Recovery

Symbol timing recovery is required in both wired as well as wireless systems and quite often employs PLL-like circuitry or algorithms. Timing errors in this process lead to (i) a loss associated with missing the correlation peak from the receive matched filter as well as (ii) additional intersymbol interference (ISI) from time-adjacent data symbols. In order to properly design the time tracking loop, we must first know the conditional error probability associated with a static timing error so that it can be used in a manner very similar to that used in (20).

In the example that we will consider, the transmit pulse shape is assumed to be a square-root raised-cosine pulse having an excess bandwidth parameter α of 0.50. The Fourier transform for such a pulse is given by

$$(23) \quad S(f) = \begin{cases} \sqrt{T_{sym}} & 0 \leq |f| \leq \frac{1-\alpha}{2T_{sym}} \\ \sqrt{\frac{T_{sym}}{2} \left[1 - \sin \left(\frac{\pi T_{sym}}{\alpha} \left(f - \frac{1}{2T_{sym}} \right) \right) \right]} & \frac{1-\alpha}{2T_{sym}} \leq |f| \leq \frac{1+\alpha}{2T_{sym}} \end{cases}$$

The receiver is assumed to use a continuous-time N=3 Butterworth filter as a close approximation for the ideal matched filter and its Fourier transform may be written as

$$(24) \quad H_{rx}(s) = \frac{1}{\left(\frac{s}{\omega_c}\right)^3 + 2\left(\frac{s}{\omega_c}\right)^2 + 2\left(\frac{s}{\omega_c}\right) + 1}$$

where ω_c is the -3 dB corner frequency in rad/sec. In the absence of noise, the individual pulse shape observed at the output of $H_{rx}(\cdot)$ may be directly computed by multiplying (23) and (24) together in the frequency domain and performing an inverse FFT. In the case where H_{rx} has BT= 0.50, this pulse shape is shown in Figure 9. In the absence of any timing error, the desired signal sample occurs coincident with the peak of the pulse as shown in Figure 9. Intersymbol interference (ISI) is clearly present as shown however, because sample values at time instants offset by $\pm kT_{sym}$ are not all zero ($k = \text{nonzero integer}$). For random data, these nonzero adjacent symbol samples create data-dependent noise at the receiver's decision making hardware thereby reducing the signal eye-opening thereby degrading system performance.

Insight into the ISI matter can be had by considering all possible sequences of 4-symbol sequences possible and the eye diagram that is observed at the receive filter output. Eye diagrams for the $\alpha = 0.50$ and 0.40 cases are shown in Figure 10 and Figure 11 respectively. The ISI and eye-closure are substantially worse for the $\alpha = 0.40$ case as

shown.

The symbol error rate for random ± 1 data can be mathematically computed by recognizing that the decision statistic consists of three components: (1) the desired signal, (2) additive Gaussian noise, and (3) data pattern-dependent ISI. Characteristic function methods may be used to combine the effects of the ISI and Gaussian noise as described in [16] leading to the symbol error rate expression with static timing error τ_e being given as

$$(25) \quad P_e(\tau_e, \sigma) = \frac{1}{2} - \frac{1}{\pi} \int_0^{\infty} \frac{\sin[\omega r(\tau_e)]}{\omega} C(\omega, \tau_e) \exp\left(-\frac{1}{2} \sigma^2 \omega^2\right) d\omega$$

Where $r(t)$ is the noise-free single-pulse shape at the receive filter output, σ^2 is the variance of the Gaussian noise at the receive filter output, and $C(\omega)$ is the characteristic function of the ISI noise. This can be shown to be given by

$$(26) \quad C(\omega, \tau_e) = \prod_{\substack{m=-L \\ m \neq 0}}^L \cos[\omega r(\tau_e + mT_{sym})]$$

Figure 9 Individual Pulse Shape at Receive Filter Output. Circled Points Reveal Pulse Response Values at Symbol-Intervals.

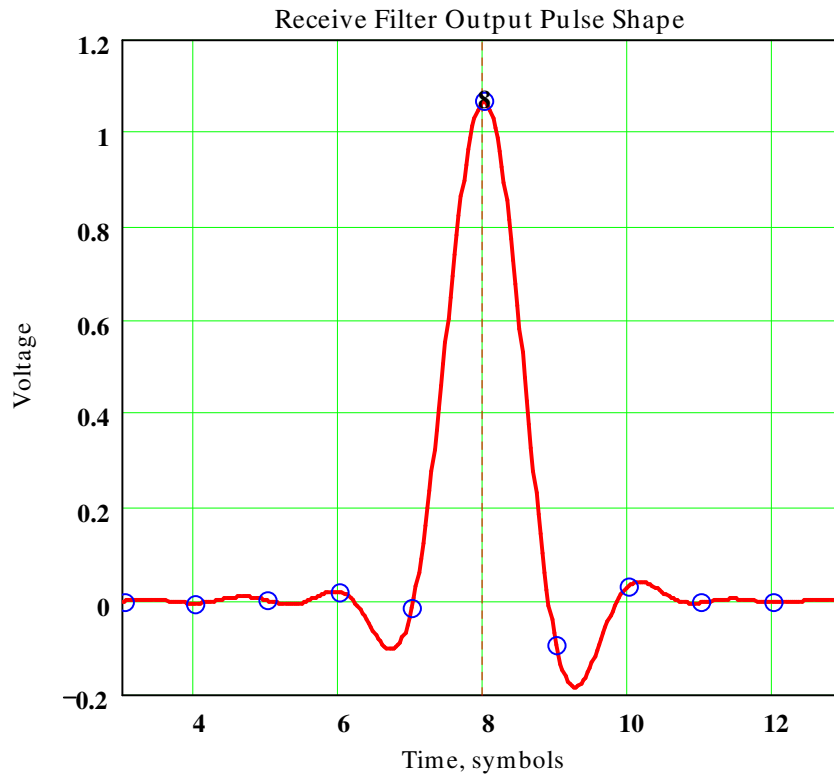


Figure 10 ISI Pattern for 16 Possible 4-Symbol Sequence with Excess Bandwidth Parameter = 0.50

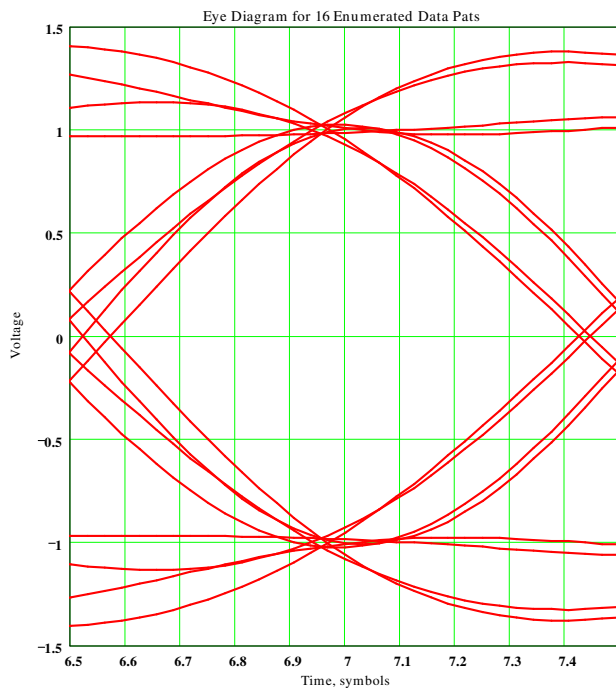
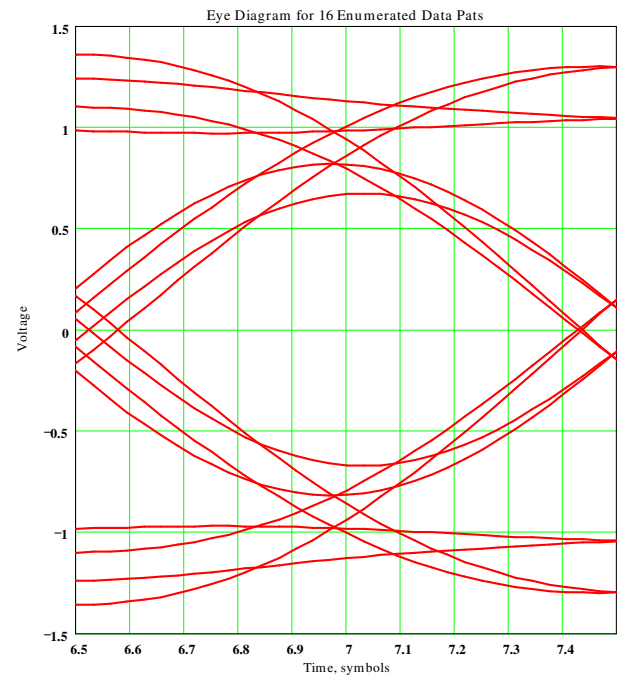


Figure 11 ISI Pattern for 16 Possible 4-Symbol Sequence with Excess Bandwidth Parameter = 0.40



The variance quantity specified in (25) can be found from the equivalent noise bandwidth of the receive filter as

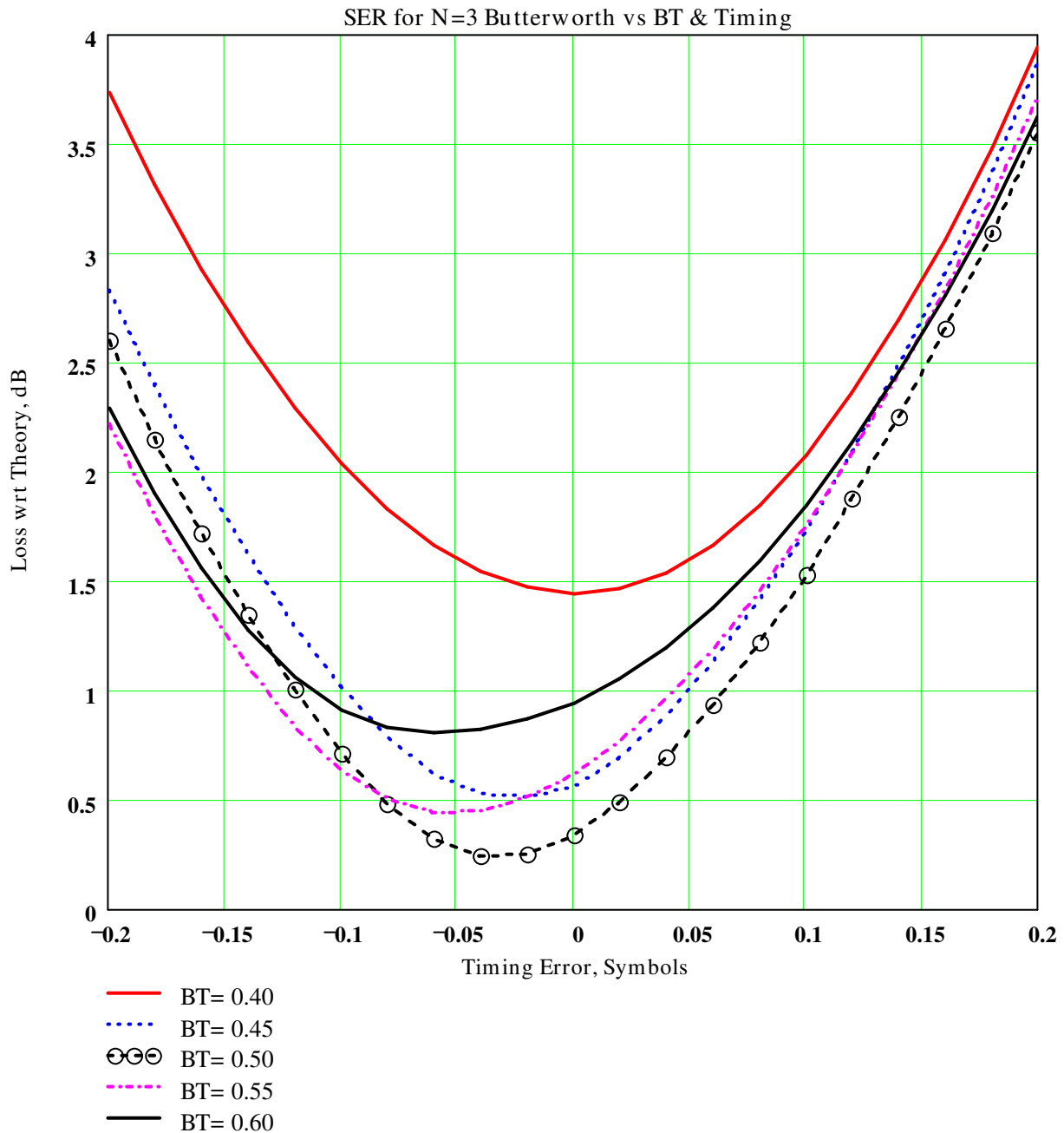
$$(27) \quad \sigma^2 = \frac{N_o}{2} \int_{-\infty}^{+\infty} |H_{rx}(j\omega)|^2 d\omega$$

where N_o is the one-sided Gaussian white noise power spectral density. Detailed calculations for these examples can be found elsewhere [17].

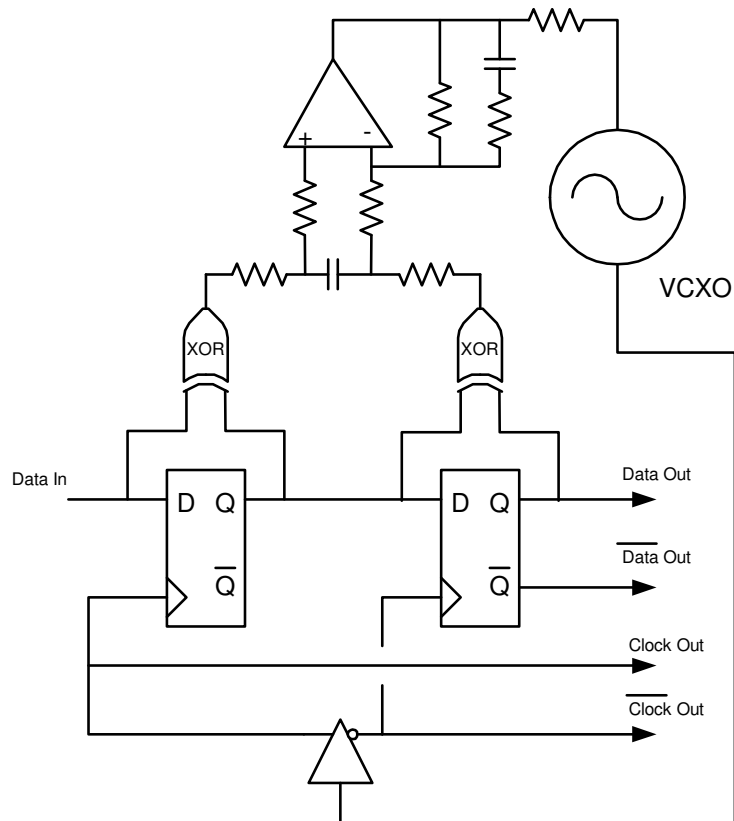
The foregoing results were used to compute the effect of timing error on symbol error rate performance as a function of the receive filter BT product as shown in Figure 12. The optimal value for best performance is $BT = 0.50$ which leads to a performance loss of only about 0.25 dB at an input E_s/N_o value of 9.6 dB which is quite remarkable. The curves shown in Figure 12 can indirectly provide the needed conditional error probability like that used in (20) thereby allowing the complete impact of imperfect PLL time-tracking behavior to be assessed.

Additional information regarding estimation theory and its application to synchronization can be found in [19].

Figure 12 Symbol Error Rate Versus Static Timing Error and Filter BT Product



In the context of hardware-based symbol timing recovery, many different types of timing error metrics are available, but one stands out in particular for very high-speed data applications in which most other detectors fall prey to meta-stability problems. This detector type was first patented by Hogge [18] and is shown here in Figure 13. This detector is rather uniquely equipped for extremely high-speed data applications and in this figure, is shown being used within a type-2 3rd-order PLL structure.

Figure 13 Hogge Clock-Recovery Circuit Within PLL Structure [18]

6 Summary

This two-part article has covered a wide range of PLL-related topics, but nonetheless space limitations precluded even mentioning other PLL-workhorses like Costas loops, joint timing and phase recovery PLLs, etc. If these articles succeeded in illustrating the versatile and pervasive aspects of the PLL concept, make a point in becoming more studious in PLLs. You will be glad that you did.

7 References

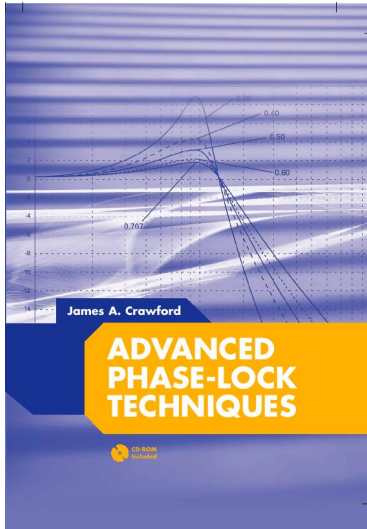
1. J.A. Crawford, *Frequency Synthesizer Design Handbook*, Artech House, 1994
2. _____, "Thoughts on Charge-Pump Phase Noise", 1999, (<http://www.siliconrfsystems.com/Papers/ChargePump.pdf>)
3. D. Banerjee, "PLL Performance", National Semiconductor
4. _____, "PLL Performance, Simulation & Design", 3rd Ed., 2003, National Semiconductor, (<http://www.national.com/appinfo/wireless/files/Deansbook3.pdf>)
5. W.P. Robins, *Phase Noise in Signal Sources*, Peter Peregrinus Ltd., 1982
6. J.A. Crawford, "U10650 Type-2 4th-Order PLL Worksheet", 24 March 2004, <http://>
7. _____, "Phase Noise Effects on Square-QAM Symbol Error Rate Performance, 2004, (<http://www.siliconrfsystems.com/Papers/Phase%20Noise%20Effects%20on%20Square%20QAM%20v1.pdf>)
8. R. Gilmore, "Specifying Local Oscillator Phase Noise Performance- How Good is Good Enough?", (<http://www.siliconrfsystems.com/Papers/U10236%20Phase%20Noise-%20How%20Good-%20Gilmore.pdf>)
9. P.O. Amblard et al., "Phase Tracking: What Do We Gain from Optimality? Particle Filtering Versus Phase-Locked Loops", March 2001
10. G. Welch, G. Bishop, "An Introduction to the Kalman Filter", March 1, 2004
11. P.F. Driessen, "DPLL Bit Synchronizer with Rapid Acquisition Using Adaptive Kalman Filtering Techniques", IEEE Trans. Comm. Sept., 1994
12. A. Patapoutian, "On Phase-Locked Loops and Kalman Filters", IEEE Trans. Comm., May, 1999
13. J.S. Lee, J.H. Hughen, "An Optimum Phase Synchronizer in a Partially Coherent Receiver", IEEE Trans. Aerospace and Electronic Systems, July, 1971
14. R.E. Ziemer, R.L. Peterson, *Digital Communications and Spread Spectrum Systems*, Macmillan, 1985
15. J.A. Bingham, *The Theory and Practice of Modem Design*, John Wiley & Sons, 1988
16. Ho, "Evaluation of Error Probability Including Intersymbol Interference", Bell System Technical Journal, Nov. 1970
17. J.A. Crawford, "U10651 SER with Timing Error", March 2004, <http://>
18. C.R. Hogge, "A Self-Correcting Clock Recovery Circuit", IEEE Trans. Electronic Devices, December 1985
19. H. Meyr, M. Moeneclaey, S.A. Fechtel, *Digital Communication Receivers Synchronization, Channel Estimation, and Signal Processing*, John Wiley & Sons, 1998
20. M.D. Srinath, P.K. Rajasekaran, *An Introduction to Statistical Signal Processing with Applications*, John Wiley & Sons, 1979
21. H.L. Van Trees, *Detection, Estimation, and Modulation Theory*, John Wiley & Sons,

1968

22. J.M. Mendel, *Lessons in Theory for Signal Processing, Communications, and Control*, Prentice-Hall, 1995

23. A. Gelb, *Applied Optimal Estimation*, The Analytical Sciences Corporation, 1996

Word Count= 3645



Advanced Phase-Lock Techniques

James A. Crawford

2008

Artech House

510 pages, 480 figures, 1200 equations
CD-ROM with all MATLAB scripts

ISBN-13: 978-1-59693-140-4

ISBN-10: 1-59693-140-X

Chapter	Brief Description	Pages
1	<i>Phase-Locked Systems—A High-Level Perspective</i> An expansive, multi-disciplined view of the PLL, its history, and its wide application.	26
2	<i>Design Notes</i> A compilation of design notes and formulas that are developed in details separately in the text. Includes an exhaustive list of closed-form results for the classic type-2 PLL, many of which have not been published before.	44
3	<i>Fundamental Limits</i> A detailed discussion of the many fundamental limits that PLL designers may have to be attentive to or else never achieve their lofty performance objectives, e.g., Paley-Wiener Criterion, Poisson Sum, Time-Bandwidth Product.	38
4	<i>Noise in PLL-Based Systems</i> An extensive look at noise, its sources, and its modeling in PLL systems. Includes special attention to $1/f$ noise, and the creation of custom noise sources that exhibit specific power spectral densities.	66
5	<i>System Performance</i> A detailed look at phase noise and clock-jitter, and their effects on system performance. Attention given to transmitters, receivers, and specific signaling waveforms like OFDM, M-QAM, M-PSK. Relationships between EVM and image suppression are presented for the first time. The effect of phase noise on channel capacity and channel cutoff rate are also developed.	48
6	<i>Fundamental Concepts for Continuous-Time Systems</i> A thorough examination of the classical continuous-time PLL up through 4 th -order. The powerful Haggai constant phase-margin architecture is presented along with the type-3 PLL. Pseudo-continuous PLL systems (the most common PLL type in use today) are examined rigorously. Transient response calculation methods, 9 in total, are discussed in detail.	71
7	<i>Fundamental Concepts for Sampled-Data Control Systems</i> A thorough discussion of sampling effects in continuous-time systems is developed in terms of the z-transform, and closed-form results given through 4 th -order.	32
8	<i>Fractional-N Frequency Synthesizers</i> A historic look at the fractional-N frequency synthesis method based on the U.S. patent record is first presented, followed by a thorough treatment of the concept based on Δ - Σ methods.	54
9	<i>Oscillators</i> An exhaustive look at oscillator fundamentals, configurations, and their use in PLL systems.	62
10	<i>Clock and Data Recovery</i> Bit synchronization and clock recovery are developed in rigorous terms and compared to the theoretical performance attainable as dictated by the Cramer-Rao bound.	52